Two-photon excitation selective plane illumination microscopy (2PE-SPIM) of highly scattering samples: characterization and application

Zeno Lavagnino,[1,2] Francesca Cella Zanacchi,[2,*] Emiliano Ronzitti [2,3] and Alberto Diaspro[1,2]

[1]*Department of Physics, University of Genoa, Via Dodecaneso 33, 16146, Genoa, Italy*
[2]*Istituto Italiano di Tecnologia, Via Morego 30, 16163, Genoa, Italy*
[3] *(currently) Wavefront Engineering Group, Laboratory of Neurophysiology and New Microscopies, Université Paris Descartes, CNRS UMR 8154, INSERM S603,45 rue des Saints Pères, 75006 Paris, France*
[*]*francesca.cella@iit.it*

Abstract: In this work we report the advantages provided by two photon excitation (2PE) implemented in a selective plane illumination microscopy (SPIM) when imaging thick scattering samples. In particular, a detailed analysis of the effects induced on the real light sheet excitation intensity distribution is performed. The comparison between single-photon and two-photon excitation profiles shows the reduction of the scattering effects and sample-induced aberrations provided by 2PE-SPIM. Furthermore, uniformity of the excitation distribution and the consequent improved image contrast is shown when imaging scattering phantom samples in depth by 2PE-SPIM. These results show the advantages of 2PE-SPIM and suggest how this combination can further enhance the SPIM performance. Phantom samples have been designed with optical properties compatible with biological applications of interest.

OCIS codes: (110.0113) Imaging through turbid media; (180.0180) Microscopy.

References and links

1. J. Huisken, J. Swoger, F. Del Bene, J. Wittbrodt, and E. H. K. Stelzer, "Optical sectioning deep inside live embryos by selective plane illumination microscopy," Science **305**(5686), 1007–1009 (2004).
2. P. J. Verveer, J. Swoger, F. Pampaloni, K. Greger, M. Marcello, and E. H. K. Stelzer, "High-resolution three-dimensional imaging of large specimens with light sheet-based microscopy," Nat. Methods **4**(4), 311–313 (2007).
3. P. J. Keller, A. D. Schmidt, A. Santella, K. Khairy, Z. Bao, J. Wittbrodt, and E. H. K. Stelzer, "Fast, high-contrast imaging of animal development with scanned light sheet-based structured-illumination microscopy," Nat. Methods **7**(8), 637–642 (2010).
4. M. Friedrich, Q. Gan, V. Ermolayev, and G. S. Harms, "STED-SPIM: Stimulated emission depletion improves sheet illumination microscopy resolution," Biophys. J. **100**(8), L43–L45 (2011).
5. F. Cella Zanacchi, Z. Lavagnino, M. Perrone Donnorso, A. Del Bue, L. Furia, M. Faretta, and A. Diaspro, "Live-cell 3D super-resolution imaging in thick biological samples," Nat. Methods **8**(12), 1047–1049 (2011).
6. C. J. Sheppard and T. Wilson, "Depth of field in the scanning microscope," Opt. Lett. **3**(3), 115–117 (1978).
7. A. Rohrbach, "Artifacts resulting from imaging in scattering media: a theoretical prediction," Opt. Lett. **34**(19), 3041–3043 (2009).
8. V. Ntziachristos, "Going deeper than microscopy: the optical imaging frontier in biology," Nat. Methods **7**(8), 603–614 (2010).
9. J. Huisken and D. Y. Stainier, "Even fluorescence excitation by multidirectional selective plane illumination microscopy (mSPIM)," Opt. Lett. **32**(17), 2608–2610 (2007).
10. R. Tomer, K. Khairy, F. Amat, and P. J. Keller, "Quantitative high-speed imaging of entire developing embryos with simultaneous multiview light-sheet microscopy," Nat. Methods **9**(7), 755–763 (2012).
11. U. Krzic, S. Gunther, T. E. Saunders, S. J. Streichan, and L. Hufnagel, "Multiview light-sheet microscope for rapid in toto imaging," Nat. Methods **9**(7), 730–733 (2012).

#180772 - $15.00 USD Received 29 Nov 2012; revised 26 Jan 2013; accepted 16 Feb 2013; published 4 Mar 2013

12. T. A. Planchon, L. Gao, D. E. Milkie, M. W. Davidson, J. A. Galbraith, C. G. Galbraith, and E. Betzig, "Rapid three-dimensional isotropic imaging of living cells using Bessel beam plane illumination," Nat. Methods **8**(5), 417–423 (2011).
13. F. O. Fahrbach, P. Simon, and A. Rohrbach, "Microscopy with self-reconstructing beams," Nat. Photonics **4**(11), 780–785 (2010).
14. W. Denk, J. H. Strickler, and W. W. Webb, "Two-photon laser scanning fluorescence microscopy," Science **248**(4951), 73–76 (1990).
15. A. Diaspro, G. Chirico, and M. Collini, "Two-photon fluorescence exitation and related thechniques in biological microscopy," Q. Rev. Biophys. **15**, 1–70 (2006).
16. J. Palero, S. I. C. O. Santos, D. Artigas, and P. Loza-Alvarez, "A simple scanless two-photon fluorescence microscope using selective plane illumination," Opt. Express **18**(8), 8491–8498 (2010).
17. F. Cella Zanacchi, Z. Lavagnino, E. Ronzitti, and A. Diaspro, "Two-photon fluorescence excitation within a light sheet based microscopy architecture," Proc. SPIE **7903**, 7903–7906 (2011).
18. T. V. Truong, W. Supatto, D. S. Koos, J. M. Choi, and S. E. Fraser, "Deep and fast live imaging with two-photon scanned light-sheet microscopy," Nat. Methods **8**(9), 757–760 (2011).
19. W. Supatto, T. V. Truong, D. De' Barrel, and E. Beaurepair "Advances in multiphoton microscopy for imaging embryos" Curr Opinion Gen. Dev (21) 538–548 (2011)
20. P. Theer and W. Denk, "On the fundamental imaging-depth limit in two-photon microscopy," J. Opt. Soc. Am. A **23**(12), 3139–3149 (2006).
21. K. Greger, J. Swoger, and E. H. K. Stelzer, "Basic building units and properties of a fluorescence single plane illumination microscope," Rev. Sci. Instrum. **78**(2), 023705 (2007).
22. A. N. Yaroslavsky, P. C. Schulze, I. V. Yaroslavsky, R. Schober, F. Ulrich, and H. J. Schwarzmaier, "Optical properties of selected native and coagulated human brain tissues in vitro in the visible and near infrared spectral range," Phys. Med. Biol. **47**(12), 2059–2073 (2002).
23. J. R. Mourant, J. P. Freyer, A. H. Hielscher, A. A. Eick, D. Shen, and T. M. Johnson, "Mechanisms of light scattering from biological cells relevant to noninvasive optical-tissue diagnostics," Appl. Opt. **37**(16), 3586–3593 (1998).
24. W. Cheong, S. Prahl, and A. Welch, "A review of the optical properties of biological tissues," IEEE J. Quantum Electron. **26**(12), 2166–2185 (1990).
25. *S. Prahl, Mie Scattering Calculator,* http://omlc.ogi.edu/calc/mie_calc.html
26. J. Debnath, S. K. Muthuswamy, and J. S. Brugge, "Morphogenesis and oncogenesis of MCF-10A mammary epithelial acini grown in three-dimensional basement membrane cultures," Methods **30**(3), 256–268 (2003).
27. B. E. A. Saleh and M. C. Teich, *Fundamentals of Photonics* (Wiley & Sons, 1991), Chap. 3.
28. J. G. Ritter, R. Veith, J.-P. Siebrasse, and U. Kubitscheck, "High-contrast single-particle tracking by selective focal plane illumination microscopy," Opt. Express **16**(10), 7142–7152 (2008).
29. J. Ying, F. Liu, and R. R. Alfano, "Spatial distribution of two-photon-excited fluorescence in scattering media," Appl. Opt. **38**(1), 224–229 (1999).
30. P. F. Mullaney and P. N. Dean, "The small angle light scattering of biological cells. Theoretical considerations," Biophys. J. **10**(8), 764–772 (1970).
31. J. Ying, F. Liu, and R. R. Alfano, "Effect of scattering on nonlinear optical scanning microscopy imaging of highly scattering media," Appl. Opt. **39**(4), 509–514 (2000).
32. C. J. Engelbrecht and E. H. K. Stelzer. "Resolution enhancement in a light-sheet-based microscope (SPIM)." Opt Lett. 10, 1477–1479 (2006)
33. J. T. Bushberg, J. A. Seibert, E. M. Leidholt, Jr., and J. M. Boone, *The Essential Physics of Medical Imaging* (Lippincott Williams & Wilkins, 2006) Chap. 10.

1. Introduction

In the last decade, light sheet fluorescence microscopy (LSFM) has become one of the largest growing techniques in optical microscopy. It combines the advantages of standard fluorescence microscopy with a remarkable optical sectioning and fast recording capability due to the confinement of the excitation process within the focal plane and to the wide-field approach, respectively [1,2]. Moreover, it significantly reduces phototoxicity and photobleaching, therefore being of particular interest for long-term experiments on living samples [3]. Thanks to these performance qualities, light sheet fluorescence microscopy (LSFM), in particular Selective Plane Illumination Microscopy (SPIM), represents an optimal tool for investigating samples up to few millimeters thick, whilst still allowing super-resolution techniques to be performed [4,5]. However, especially when imaging large biological samples, aberrations deriving from the interaction between light and matter can appreciably affect the image formation process.

In particular, the scattering of light travelling across the sample is one of the main causes of aberrations that sometimes compromise overall performance [6–8]. Scattering is induced

#180772 - $15.00 USD Received 29 Nov 2012; revised 26 Jan 2013; accepted 16 Feb 2013; published 4 Mar 2013

by a refractive index mismatch within the sample and can lead to different light excitation phenomena, causing a spread or a deviation of the excitation volume.

To eliminate such aberrations, different approaches have been attempted in LSFM. One of these is the multi-directional SPIM (mSPIM) technique, in which the imaging capabilities of the system are enhanced thanks to a double excitation path and multi-view reconstruction [9–11]. Recently, different illumination patterns, i.e. Bessel beam [12], have been proposed as suitable solutions for enhancing the penetration imaging capability in thick samples thanks to their self-reconstruction qualities [13].

Additionally, Two-Photon Excitation (2PE) has become a golden standard for reducing sample-induced aberrations, thanks to the use of red-shifted wavelength and the intrinsic excitation confinement [14,15]. Within this scenario, the combination of light sheet based fluorescence microscopy and two-photon excitation has been shown in conventional SPIM [16,17] and successfully applied to Drosophila imaging in a Digital Scanned Laser Microscopy (DSLM) architecture [18,19].

Nevertheless, despite the higher wavelengths used, which should allow to reduce scattering-induced aberrations of the excitation volume,, 2PE could still be prone to a shift of the peak of the excitation intensity distribution and a consequent undesired excitation of the region close to the surface [20]. In fact, similarly to conventional 2PE microscopy, a distortion of the excitation volume can still affect the imaging performance of selective plane illumination, thus limiting the depth-penetration capabilities of such a system.

The aim of this work is to underline the real advantages provided by TPE-SPIM when imaging thick scattering samples through a detailed study of the effective excitation distributions.

2. Materials and methods

The Single Plane Illumination Microscope setup (Fig. 1(A)) used here derives from the "classical" SPIM which was developed by Stelzer et al. [21]. The laser lines coupled to the system are a Coherent Chameleon Ultra 2 (pulse width 140 fs across the wavelength tuning range, repetition rate 80 MHz) which can perform two-photon excitation and a Coherent 488 nm laser for single photon excitation.

The laser beam is directed to a shaping unit which allows the size of the beam incident on the cylindrical lens to be changed in order to tune across the dimensions of the excitation light sheet.

The focal distance of the cylindrical lens used is 200 mm both for single photon and two-photon excitation (Thorlabs LJ1653L1-A and Thorlabs LJ1653R-B, respectively).

The illumination objective is a Nikon 10x NA 0.3. Fluorescence is gathered by a water dipping Leica 20x NA 0.5 oriented 90° relative to the illumination objective. Dichroic mirrors (Chroma T505LP for 1P, Semrock FF670 SDi 01 for 2P) and filters (Semrock Brightline Fluofilter 525/50, Chroma SP680) are combined to obtain the best spectral selection of the signal impinging the CCD target (Andor IXon DU-897E-CS0BV).The calibrated phantom samples were made from agar gel (Sigma Aldrich, low melting point, diluted 2%) to minimise refractive index mismatch, since the sample is inserted in a chamber filled with aqueous medium, with a solution of FITC dextrans –1 mg/10 ml- (500 KDa, Sigma Aldrich) entrapped in the agarose network.

The volume of the capillary tubes (Socorex) in which the phantom samples are inserted are 60 – 100 µl. Only a portion of the volume was used, thus leading to a phantom sample with a cylindrical shape, 3mm (height) x 2mm (diameter).

Following a calculation within the Mie Theory frameset, different scattering coefficients were obtained for the phantom samples when variable amounts of non-fluorescent microspheres (d = 1.03 micron, Nist, Polysciences) were added. In particular, to obtain a scattering coefficient of $5mm^{-1}$, $10mm^{-1}$, $30mm^{-1}$ and $50mm^{-1}$, concentrations of 3.64, 7.28, 22.75 and 36.4 particles/µl were used, respectively. These scattering coefficients were chosen

#180772 - $15.00 USD Received 29 Nov 2012; revised 26 Jan 2013; accepted 16 Feb 2013; published 4 Mar 2013

to represent different scattering tissues such as bladder, muscles, brain and cellular aggregates [22–24]. Reduced scattering coefficients ($\mu_S' = \mu_S(1-g)$, where g represents the anisotropy factor, which equals the average cosine of the scattering angle values) are 2,5 cm^{-1}, 6 cm^{-1}, 9 cm^{-1} and 10 cm^{-1}, according to g values, 0.95, 0.94, 0.97 and 0.98 respectively for the scattering coefficients mentioned above.

The experiments were performed on the phantom samples, rotating the cylindrical lens by 90 degrees, by imaging the light sheet intensity distribution on a CCD target (see scheme in Fig. 1(B,C)). Phantom samples were made from a low melting point agarose gel in which different concentrations of beads were diluted to obtain the desired tunable optical properties, according to Mie calculations [25]. Samples with 4 different scattering coefficients mimicking the optical behavior of different classes of interesting biological specimens were made. So far, we have performed experiments at different propagation depths within the sample (respectively 400, 600 and 800 μm within the sample), keeping the distance from the detection objective constant.

As regards biological specimen, MCF10A immortalized human mammary cells were cultured in 3D growing conditions on a Matrigel layer (BD Biosciences) [26]. The resulting mammary cell spheroids were then fixed in 4% PFA for 15 mins. Nuclear staining was performed in order to incubate the sample for 15 mins in Hoechst 33342 (Invitrogen) (1μM in dH_2O). Finally, the labeled spheroids were then embedded in 1.5% low melting-point agarose gel (Invitrogen) for imaging purposes.

#180772 - $15.00 USD Received 29 Nov 2012; revised 26 Jan 2013; accepted 16 Feb 2013; published 4 Mar 2013

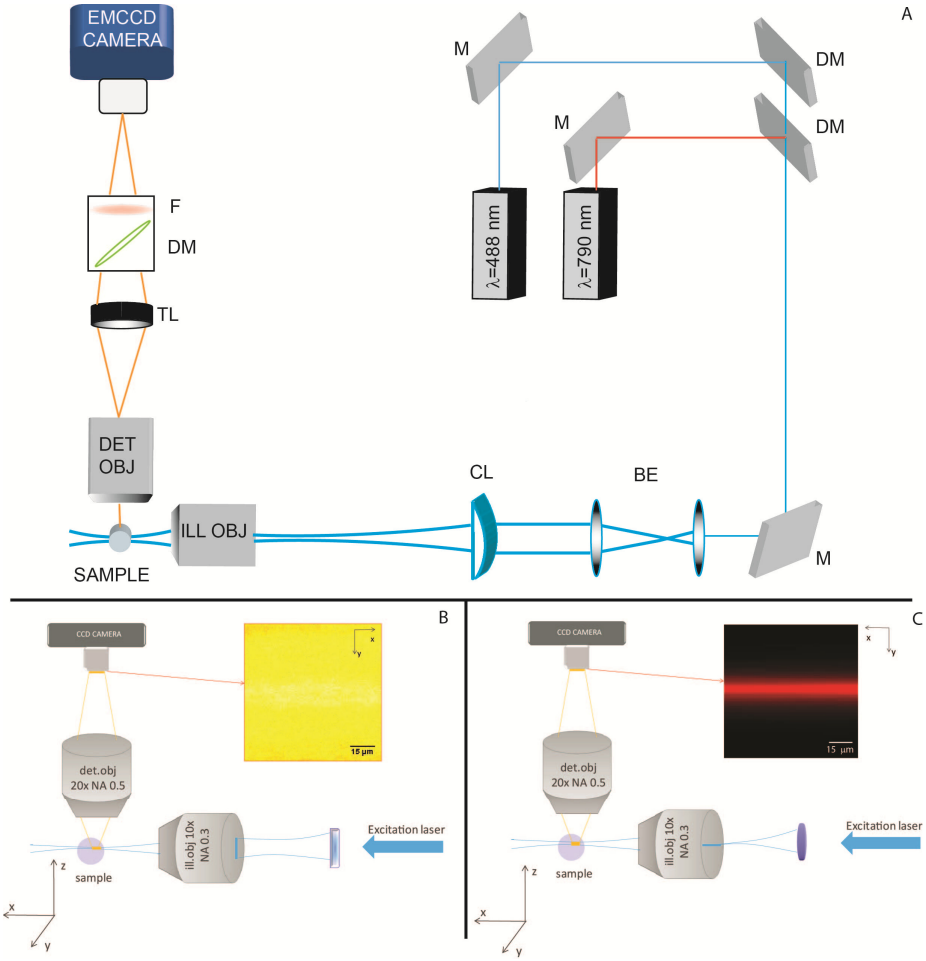

Fig. 1. Scheme of the Selective Plane Illumination Microscope (A) adapted from [5]. Figure B and fig. C show the adaptation of the system for the experimental measurements. With the cylindrical lens in its standard position, a light sheet is produced in the focus of the objective lens, and a homogeneous fluorescent image of the phantom sample is produced on the CCD Camera (B). Rotating the cylindrical lens by 90 degrees, the axial section of the intensity excitation distribution appears on the CCD sensor.

3. Assumptions

The most significant feature of a selective plane illumination microscope is its intrinsic optical sectioning image formation capability. The thickness of the illuminating light sheet and the numerical aperture of the detection objective are governing the axial resolution. Sample- induced aberrations of the light sheet excitation distribution play a key role in reducing image quality and also hamper the optical sectioning capability. We consider the light sheet as focused by an illumination objective and a Gaussian intensity distribution orthogonal to the propagation direction is produced.

Since the light sheet can be assumed [27] to be focused along one axis, the homogeneneous region of the light sheet lies within the focal depth - twice the Rayleigh range - approximated by a rectangle [28]. The thickness and the homogeneous light sheet region can be varied as a function of various parameters, such as the dimension of the incident beam, the focal length of the cylindrical lens, the NA of the illumination objective and the medium in which the light sheet travels.

#180772 - $15.00 USD Received 29 Nov 2012; revised 26 Jan 2013; accepted 16 Feb 2013; published 4 Mar 2013

An effective estimation of light sheet geometry can be obtained by analyzing the illumination intensity distribution in reflection mode. To this end, a mirror is inserted at 45 degrees between the illumination and the detection objective.

To compare the scattering effects arising under 1P and 2P configurations, the same illumination conditions were set resulting in comparable light sheet spatial distributions. The elliptical Gaussian excitation intensity distribution modified by the scattering loss can be derived from:

$$I_{1P}(x,y,z) = I_0(x)e^{(-\frac{y^2}{2\sigma_y^2}-\frac{z^2}{2\sigma_z^2})}e^{-\mu_s x} \quad (1)$$

where σ_y and σ_z are the standard deviations along their respective axes and μ_s represents the scattering coefficient.

Similarly, 2PE intensity distribution, which is proportional to the square of the illumination intensity distribution ($I_{2P} \alpha I_{1P}^2$), can be described by:

$$I_{2P}(x,y,z) \propto I_0^2(x)e^{(-\frac{y^2}{\sigma_y^2}-\frac{z^2}{\sigma_z^2})}e^{-2\mu_s x} \quad (2)$$

The excitation intensity distribution, at a coordinate deep inside the medium, decays exponentially according to the increase of the scattering coefficient of the specimen. Nevertheless, the focal peak tends to shift backwards [29].

According to the scattering coefficients and excitation wavelengths considered, absorption is usually negligible [22,24] and scattering effects are considered along the direction of the propagating excitation beam, taken within the small angle approximation [30]. The preparation of the phantom samples implies that there's no local refractive index variation, leading to a homogeneous scattering condition. This means that, at every coordinate in the phantom sample space, a uniform beads concentration can be considered leading to a homogeneous scattering coefficient inside the sample itself. For this reason the optical properties of the phantom scattering samples are controlled using different concentration of microspheres having diameters larger than the excitation wavelength used (thus, the relation between the optical properties and the concentration can be predicted according to Mie theory).Although scattering and wavefront distortion both occur in biological tissues, light propagation in microscopy is often modeled as purely scattering, described in terms of modulation of the power of ballistic photons [20]. This leads to the attenuation of the ballistic laser power with tissue depth, an enlargement of the Point Spread Function and generation of out of focus 2P excitation [20]. Even if these phantom samples cannot perfectly mimic the optical properties of a real biological sample, they are an optimal approximation for understanding the behavior of the light sheet in the presence of scattering and the performance characterization of a light sheet microscopy architecture based on deep imaging in scattering tissues.

4. Results and discussions

In order to define the possible advantages of priming 2PE within a lightsheet, we performed a series of measurements of the light sheet excitation distribution by imaging an immobile fluorescent sample made from FITC dextrans molecules embedded in 1,5% agarose gel.

System performance in the presence of a thick scattering sample was assessed by analyzing excitation light sheet uniformity in the field of view. It was previously shown that while imaging deep in a scattering sample, a significant amount of fluorescence can be generated at the sample surface, thus limiting imaging performance [20,31]. A similar effect can also be expected in Selective Plane Illumination Microscopy (SPIM), thus producing a shift of the uniform excitation intensity distribution (see Fig. 2) region where image formation usually takes place. We analyzed the excitation intensity profile along the direction of light

#180772 - $15.00 USD Received 29 Nov 2012; revised 26 Jan 2013; accepted 16 Feb 2013; published 4 Mar 2013

propagation (Fig. 2(D)) to test excitation homogeneity in the entire Field Of View (FOV), both in single and two-photon configurations. The same measurement was made on phantom samples with different scattering coefficients (from 5mm^{-1} to 50mm^{-1}) in order to investigate the influence of the optical properties of the sample. The geometry of the effective light sheet regions, i.e. where light sheet intensity can be considered as uniformly distributed, was evaluated by fitting the related excitation intensity profiles with a Gaussian curve. The region within the 1/e^2 of the fitted curve can be considered as the uniform intensity area [32]. The data were analyzed and the peak values from the excitation intensity distribution profiles were identified, according to Eqs. (1) and (2). Figure 1(D) shows how the measured excitation intensity distribution for single photon (1P) excitation and two-photon excitation (2P) looks like on the CCD camera in case of homogeneously low scattering phantom sample (scattering coefficient = 5 mm^{-1}).

Results for the same phantom sample mimicking the optical properties of biological tissues confirmed that in both excitation configurations, the uniform excitation intensity region that is expected to be in the focal region of the objective, is shifted towards the illumination lens position, thus generating a less uniform region for the field of view. In particular, this effect becomes more evident when imaging depth increases. Experiments were performed at increasing illumination depths within the phantom sample: 400, 600, 800 μm. The travel along the detection path within the phantom sample remains constant (150 μm). Excitation wavelengths are 488 nm for 1P and 790 nm for 2P.

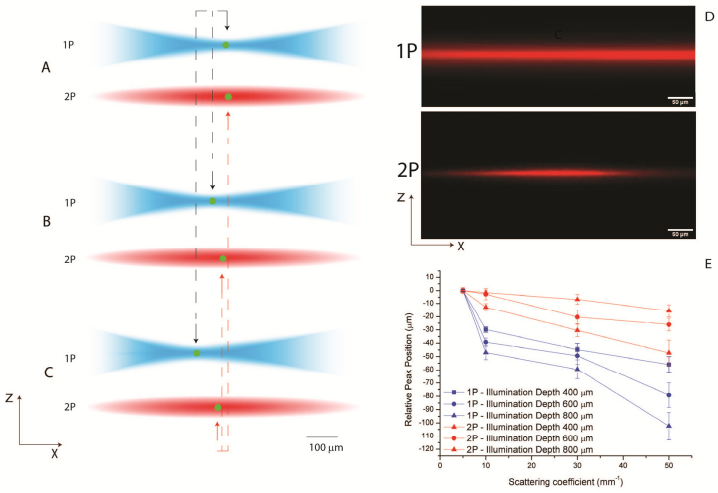

Fig. 2. Experiments performed on various phantom samples mimicking the different optical properties of biological tissues (5, 10, 30, 50 mm^{-1} respectively), considering the intensity excitation profile in the direction of propagation. Schematic representation (A-C) of the peak shift (green dot) of the excitation intensity distribution for single photon excitation (blue) and two-photon (red) excitation configurations. The arrows underline how the peak tends to shift back from the ideal case. While keeping constant the travel within the sample in the detection path (150μm) and varying both illumination depth and the scattering properties of the phantom sample, we were able to measure a significant shift for the single photon excitation configuration with respect to the two-photon configuration. D shows an example of the axial section of the measured intensity excitation distributions for the 1P and 2P excitation lightsheets for a phantom sample with 5 mm^{-1} scattering coefficient at 400 μm illumination depth. E shows the relative peak position of the uniform region with respect to the supposed focus (in a non-scattering sample) for single photon excitation at different illumination depths (400,600 and 800μm deep within the sample) while increasing the scattering coefficient of the phantom sample. 2PE allows the shift of the uniform region to be reduced. Excitation Wavelengths: λ = 488 nm (1P) and λ = 790 nm (2P) Intensity used in 1P experiments: I = 0.13 kW/cm^2; Intensity used in 2P experiments: I = 19.78 kW/cm^2. Detection Objective: Leica 20x, NA 0.5.

#180772 - $15.00 USD Received 29 Nov 2012; revised 26 Jan 2013; accepted 16 Feb 2013; published 4 Mar 2013

The analyzed data reveal, a significant scattering effect in the propagation direction of the 1P intensity excitation distribution. This produces a significant back-shift of the uniform intensity region as opposed to the ideal peak position.

According to the Gaussian excitation intensity distribution reported in Eqs. (1) and (2), we fitted the measured excitation intensity distribution related to each scattering coefficient in order to obtain the value of the peak of the distribution. All 0.95 or above reduced R^2 were considered in order to verify the goodness of the fit.

In Fig. 2(E) three different curves related to each illumination depth considered (400, 600 and 800 μm), plotting the relative peak position compared to the ideal case of the values obtained by the theoretical fit.

As expected, as the scattering coefficient of the phantom sample increases, so the back shift of the uniform intensity region becomes more pronounced. The shift of the peak depends also with the increased illumination depth, in agreement with the theoretical predictions showed in Eqs. (1) and (2).

Table 1 reports the shift (shown in Fig. 2(E)) in terms of distance (μm) from the ideal focus (i.e. the focal plane where the uniform intensity region should be in the case of an ideal sample) when light is focused in a phantom sample with scattering coefficient 50 mm^{-1}, mimicking the optical properties of cells aggregates [23].

Table 1. Summary of the values obtained from the relative shift of the excitation intensity distributions peaks for both excitation schemes. Scattering coefficient is 50 mm^{-1}.

Illumination depth	Distance from ideal Peak Position 1PE	Distance from ideal Peak Position 2PE
400 μm	56 ± 5.9 μm	15.6 ± 4.6 μm
600 μm	79.2 ± 9.2 μm	26 ± 4.8 μm
800 μm	102.4 ± 10.4 μm	47.2 ± 9.5 μm

In the 2PE configuration, the back-shift of the uniform intensity region is greatly attenuated thus improving the imaging of thick scattering specimens under single plane illumination regime. Despite the fact that scattering effects play a significant role in inducing aberrations in the light sheet excitation profile, the use of two-photon excitation is a valuable improvement in the uniformity of the excitation profile as it reduces the shift of the intensity peak when compared with 1PE. For example, with an illumination depth of 800 μm and a scattering coefficient of 50 mm^{-1}, the shift is significantly lower (around 46%) than in the single photon excitation configuration.

We also show the 1PE vs. 2PE comparison of the extension of the uniform region (as described in section 2 and 4 [32],) responsible for the useful FOV at different scattering coefficients (Table 2) at an illumination depth of 400 μm. The scattering coefficients were selected in order to range from a quasi-transparent configuration (scattering coefficient of 5 mm^{-1}), to a dense scattering sample (scattering coefficient of 50 mm^{-1}).

Table 2. Summary of the dimensions of the uniform intensity region within the exciting light sheet. The data shown are the mean values of 15 measurements made on calibrated samples. In the single photon excitation configuration, the area of uniformity reduces significantly by approximately 40 microns, while in the two photon excitation configuration there is no significant variation. This means that the two photon excitation light sheet is preserved more while travelling in deep scattering samples. Data refer to an illumination depth of 400μm.

	Transparent sample (5 mm^{-1})	Scattering sample (50 mm^{-1})
1P uniform light sheet region	428.93 ± 16.34 μm	389.3 ± 20.24 μm
2P uniform light sheet region	292.81 ± 13.66 μm	290.93 ± 19.34 μm

#180772 - $15.00 USD Received 29 Nov 2012; revised 26 Jan 2013; accepted 16 Feb 2013; published 4 Mar 2013

The loss of the uniform excitation region in terms of width is less than 1% in 2PE, while for single photon excitation it is reduced by 10%. This result confirms the fact that two-photon excitation is an optimal way of reducing scattering effects and distortions while imaging highly scattering samples in depth, which would otherwise be greatly compromised under 1PE. Increasing the illumination depth results in a reduced light sheet uniform region, because of the exponential decay shown in Eqs. (1) and (2).

Furthermore, signal to noise ratio measurements made on fluorescent beads were performed to accurately determine the imaging performance of the system.

Figure 3 shows images of fluorescent beads (d = 0.17 μm) embedded in different phantom samples with increasing scattering coefficient performed under single photon excitation (λ = 488 nm)and two-photon excitation (λ = 740 nm). Illumination depth is set at 600 μm within the sample. For these experiments, we used non fluorescent phantom samples made by agar gel with the very same concentration of non fluorescent beads we used to get 5, 10, 30, 50 mm^{-1} scattering coefficients. The concentration of fluorescent beads is low enough not to change the optical properties of the phantom samples. Moreover, the refractive index of the fluorescent beads is equal to the refractive index of the scatterers used to tune the optical properties of the system, so they can still be considered as homogeneously scattering.

As reported in Fig. 3, increasing the scattering properties of the phantom sample, the collectible signal from the beads drastically decreases and the background starts to become relevant. Nevertheless, 2PE allows better signal to noise ratio while imaging a highly scattering phantom sample in depth.

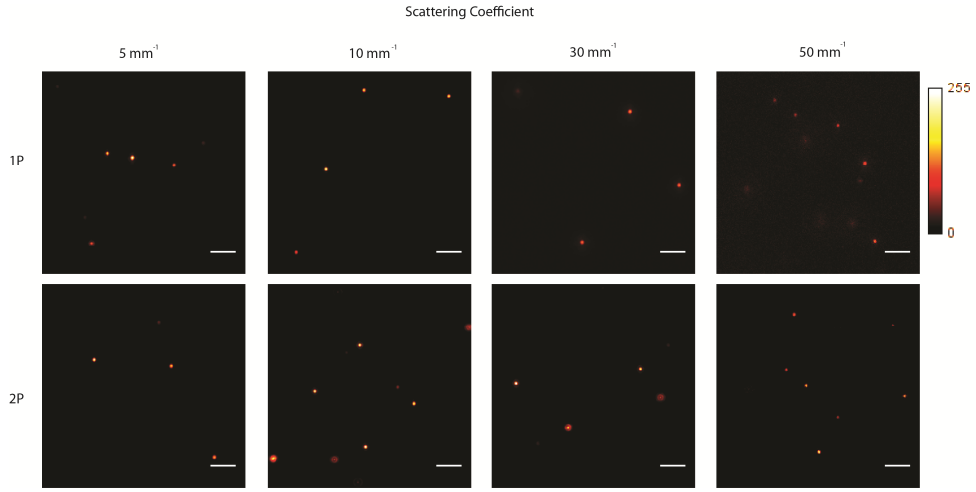

Fig. 3. Images of different homogeneously scattering phantom samples with fluorescent beads (diameter = 0.17 μm) by means of single photon and two-photon excitation SPIM. Increasing the scattering coefficient within the sample, it is possible to appreciate how signal to noise ratio in 2PE-SPIM degrades much less in comparison to the single photon case. All images are acquired at 600 μm illumination depth within the samples. Scale bar is 5 μm. Detection objective Leica HCX APO L U-V-I 12 40X, NA 0.8.Additional magnification introduced:2,5X to get a total magnification of 100X. Intensity used in single photon experiments: I = 0.11 kW/cm^2; intensity used in 2P experiments: I = 19.23 kW/cm^2

Signal to Noise Ratio (SNR), can be defined as SNR = μ/σ, where μ is the average of the signal, or meanpixel value and σ is the standard deviation of the pixel values over a given neighborhood. As an example, the ratio was measured in a phantom sample mimicking the optical properties of cell aggregates or mammary cell spheroids (scattering coefficient 50 mm^{-1}). Under 2PE the ratio is about 6.18 degrading to 4.1 for 1PE, 600 μm deep in the specimen. According to the Rose criterion [33], which states that an SNR of at least 5 is needed to be able to distinguish image features at 100% certainty, it is clear how 2PE is able

#180772 - $15.00 USD Received 29 Nov 2012; revised 26 Jan 2013; accepted 16 Feb 2013; published 4 Mar 2013

to improve the imaging capabilities of the system in case of depth imaging of highly scattering samples.

These results are able to characterize the performance of a SPIM system in presence of a thick scattering sample both in single and two-photon excitation. But even if the phantom samples adopted represent a good model for a thick sample, it is important to verify the performance of such a system while imaging a real thick biological specimen.

To this end, MCF10A cell spheroids grown under 3D basement membrane culture conditions have been imaged under 2PE SPIM, in order to show the imaging capabilities of a 2PE-SPIM in a thick sample with around 50 mm^{-1} scattering coefficient. Nuclei of cells were stained with Hoechst 33342 (Invitrogen) and imaged by means of 2PE-SPIM (see Fig. 4(A,B)). Optical sectioning capabilities of 2PE-SPIM allows plane by plane imaging (see Fig. 4(A)) through the sample, z space = 1μm, and the three dimensional reconstruction of the entire cellular spheroid (see supplementary movie). Maximum projection image is shown in Fig. 4(B).

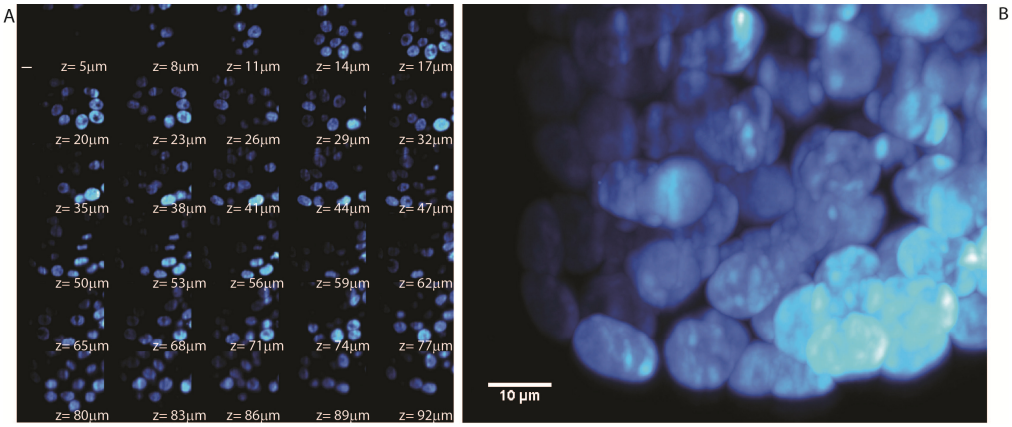

Fig. 4. Z-stack of mammary epithelial acini (zstep 1 μm) has been acquired (see Suppl. Media 1). Only representative planes within the cell spheroids (spaced 3μm) are shown (A). Scale bar: 10 μm . Maximum intensity projection of the entire volume (B). Excitation wavelength λ = 750nm, I = 54.94 KW/cm^2. Objective lens: HCX APO L U-V-I 40x/0.8 WATER.

5. Conclusion

This paper sets out to improve knowledge and comprehension of scattering effects both in 1PE and 2PE SPIM.

Experiments were performed on calibrated samples, mimicking the various optical properties of some biological samples of interest, such as bladder, muscle, brain and cell aggregates [22–24]. As expected, the results show how two-photon excitation improves the performances of a lightsheet microscope while imaging scattering samples in depth. Characterization was performed in terms of maintenance of the uniformity of the excitation intensity distribution and the signal-to-noise ratio. Experiments were carried out at different illumination penetration depths in order to check whether the excitation lightsheet distorts due to light-sample interaction and if significant fluorescence can be generated far from the theoretical focus of the uniform intensity region and 2PE SPIM 3D imaging of mammary cell spheroids was reported. Considering the high scattering coefficient, we found that the two-photon excitation lightsheet gives improved contrast while imaging deeper and deeper in a thick sample, thus attracting attention once again to the unique features that a single-plane illumination microscope, coupled with a pulsed laser performing two-photon excitation, demonstrates while imaging thick scattering samples. Since an improved comprehension of the mechanisms relative to cellular and intracellular interactions requires cellular aggregates, organs and tissues to be studied more than isolated cells, we believe that this characterization

#180772 - $15.00 USD Received 29 Nov 2012; revised 26 Jan 2013; accepted 16 Feb 2013; published 4 Mar 2013

and approach could be an interesting starting point for the design and performance of new experiments in cellular and molecular biology.

Acknowledgments

The authors would like to thank Mario Faretta and Laura Furia (Department of Experimental Oncology, European Institute of Oncology, Milan, Italy) for their support in preparing the mammary cell spheroids, and Giuseppe Vicidomini (Istituto Italiano di Tecnologia, Genoa, Italy) for helpful discussions.

#180772 - $15.00 USD Received 29 Nov 2012; revised 26 Jan 2013; accepted 16 Feb 2013; published 4 Mar 2013